AD-A145 801 NUMERICAL SIMULATIONS OF COMPLIANT MATERIAL RESPONSE TO 1/1
TURBULENT FLOW REVISION 1(U) LAWRENCE LIVERMORE
NATIONAL LAB CA A C BUCKINGHAM ET AL. AUG 84
UNCLASSIFIED UCRL-89400-REV-1 N00014-83-F-0010 F/G 13/10.1 NL

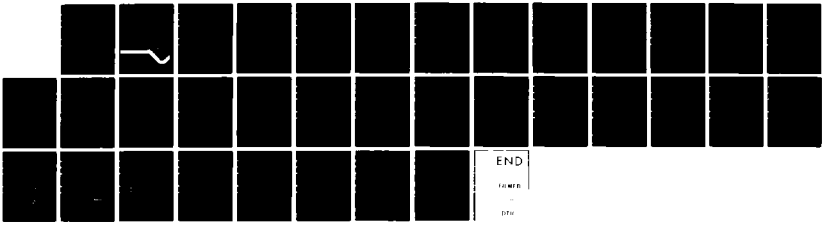

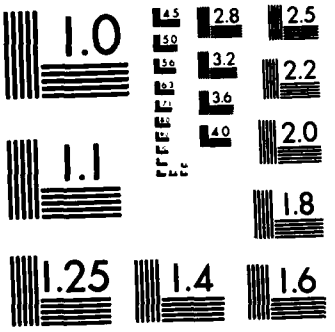

UCRL- 89400
PREPRINT
Revision 1

NUMERICAL SIMULATIONS OF COMPLIANT MATERIAL RESPONSE TO TURBULENT FLOW

Alfred C. Buckingham
Mary S. Hall
Ramsey C. Chun

This paper was prepared as a revision to
AIAA Paper No. 84-0537 for publication in the
AIAA Journal

August 1984

AIAA Log. No. J14773

Numerical Simulations of Compliant Material Response to Turbulent Flow*

Alfred C. Buckingham**, Mary S. Hall**, and Ramsey C. Chun†

Lawrence Livermore National Laboratory, Livermore, CA 94550

Abstract

Homogeneous and internally structured material coatings are studied numerically as candidates for drag and turbulence generated noise reduction on submersible hulls. Dynamic motions of compliant surfaces may conceptually interrupt random turbulent motions, reducing the turbulent interface stresses and absorbing turbulent energy, and consequently reducing the turbulence at the flow/coating interface. Time dependent, two and three dimensional Monte-Carlo turbulent pressure field models, and interactive Navier-Stokes pseudo-spectral methods are used to represent the unsteady flow, while finite element methods are applied to represent a variety of homogeneous, layered, and internally structured material coatings. The influence of added mass and in-depth overburden on the material response in ocean water is discussed. Promising compliant material coatings include sandwiches of soft, homogeneous layers between thin, stiffer elastic materials and internally structured coatings combining streamwise ribs, and spanwise voids separated by stiff elastic supporters imbedded in soft yielding viscoelastic layers.

*Work performed under the auspices of the U.S. Department of Energy by Lawrence Livermore National Laboratory under contract #W-7405-Eng-48 and supported by the Department of the Navy, Office of Naval Research under contract #N000-14-83-F-0010.

**Physicist, Theoretical and Applied Mechanics, H Division, Physics Department, Associate Fellow, and Member AIAA, respectively.

†Research Engineer, Engineering Mechanics, Nuclear Test Engineering Division, Engineering Department.

I. Introduction

After the Second World War interest in the possibilities of reducing drag through the use of compliant coatings was stimulated by study of the summary efficiency of mammals, particularly porpoises. Simulated skin coatings were developed and tested in the United States by M. O. Kramer in the 1950's and 1960's.[1,2] More recently, experimental USSR results indicate that significant reductions in turbulent skin friction drag are obtained through use of thin, elastically deforming surface coatings.[3] Unfortunately, the promising experimental results, have not been independently and substantially reproduced. The issue remains open.

Our present investigations focus on compliant coatings that exhibit favorable dynamic response to both laminar and turbulent boundary layer motions. Favorable response is that associated with reduction of skin friction drag, in our discussion. Identification of the fundamental fluid/solid dynamic coupling mechanisms having a potential for reducing skin friction drag is a primary goal. We emphasize materials and coatings whose characteristics can be altered by passive changes to internal structure, or composite material stiffness, or dynamic variations in internal stress, or by wall heating. Such coatings should be effective over a useful range of flow conditions, rather than being inherently specific to a single flow condition.

We also emphasize the effects of the added mass associated with submerged coating response. In addition, we have extended our previous analyses in order to consider three-dimensional flow distributions actively forcing three dimensional coating surfaces and we have initiated study of direct, interactive dynamic coupling between the responding surface and a surface-altered flow field. All of the calculations described here were processed on CRAY I computers.

Initial simulations of material response are non-interactive between fluid and solid regimes. Instead, the surface excitations are independently forced by modeled random space/time turbulent pressure distributions to obtain information on material response characteristics. These surface excitation simulations, mimic a turbulent pressure field on a non-compliant flat plate. These are generated by application of the Ash-Khorrami Monte-Carlo turbulent pressure field model.[4,5] These computations, albeit non-interactive, are useful for screening relative response influence of materials, material properties, composites, and internally structured coating candidates. We thereby reduce the number of candidate coatings and flow conditions that need to be considered in subsequent fully interactive fluid-solid coupling simulations. The utility of non-interactive procedures in this screening process is particularly evident in analyses of the isolated influences of overburden in ocean depth studies, virtual mass-surface displacement modulation, and three-dimensional influences relative to the theoretically more familiar two-dimensional, plane strain influences.

For direct fluid/solid interactions, Navier-Stokes flow simulations are used. We apply a pseudo-spectral method based on Orszag and Kells[6] and Orszag and Patera,[7] later extended to include small displacement rate influences of linearized surface response.[8] Flow instabilities of the Tollmein-Schlichting form are impressed on otherwise stable viscous profiles. The influence of detailed solid coating dynamic compliance is traced in the subsequent growth or reduction of the viscous instabilities.

II. Simulations & Conditions

Finite Element, Procedures

For the compliant coating materials response simulations we apply a discretized procedure to simulate the response of composite materials and internally structured

coatings. To follow high frequency and relatively large deformation motions, we adapt both implicit and explicit two–dimensional and three–dimensional versions of the Hallquist finite element codes.[9,10] In some of our computations, explicit–in–time finite element computations are applied since the Courant–stable time interval for elemental response is of the same order (or larger) than the virtual, implicit time interval sampling rate required for the response frequency range of interest. Having established the explicit fluid/solid time data base associated with the dynamic response of representative coatings, we are able to develop interpolation and time–sequencing (sub cycling) rules and algorithms for automatic fluid/solid coupling procedures in subsequent, efficient implicit code applications.

Discussion of the finite element procedure is based on the implicit, iterative formulation, for generality. The unsteady dynamical problem is represented as an incremental (Δ) perturbation to the equilibrium state. A lumped or consistent mass matrix relationship describes the instantaneous perturbation at an incremental time epoch, N + 1, based on a solution (or initial conditions) at a previous time epoch, N,

$$\underset{\sim}{M}\,\overset{\bullet\bullet}{\underset{\sim}{d}}^{(N+1)} + \underset{\sim}{D}(\underset{\sim}{d}^{(N)} + \alpha\Delta\underset{\sim}{d}^{*(N)})\,\overset{\bullet}{\underset{\sim}{d}}^{(N+1)} + \underset{\sim}{K}_t(\underset{\sim}{X}^{(N)})\;\Delta\underset{\sim}{d}_0$$

$$= \underset{\sim}{P}(X^{(N)})^{(N+1)} - \underset{\sim}{F}(\underset{\sim}{X}^{(N)}) \,, \qquad (1)$$

where $\underset{\sim}{M}$ is the lumped mass matrix, $\underset{\sim}{d}$ is the nodal displacement vector relative to coordinate vector, $\underset{\sim}{d} = (\underset{\sim}{X}^{(N+1)} - \underset{\sim}{X}^{(N)})$, $\underset{\sim}{K}_t$ is the material property dependent, tangent stiffness matrix, $\Delta\underset{\sim}{d}^{*(N)}$ is the iteratively estimated displacement increment for this load step while $\Delta\underset{\sim}{d}_o$ is the prescribed displacement increment for the implicit time increment, $\Delta t = t^{N+1} - t^{N}$. P is the external loads vector based on the applied loading at epoch N+1 but on the geometry at epoch N. The stress divergence vector, $\underset{\sim}{F}$, is based on the

displaced state and stresses at load step N. Time rates of change and accelerations of the displacement vector are symbolized by the single and double dot superscripts, respectively.

The Rayleigh damping matrix is iteratively evaluated as linear combination of mass and stiffness matrices.

$$\underset{\sim}{D} = \alpha \underset{\sim}{M} + \beta \underset{\sim}{K}_t \ , \tag{2}$$

where α and β are user–prescribed constant scale factors with α typically less than or equal to 1/2 and β typically equal to 1/4. Time evolution of equation (1) involves use of an unconditionally stable, one step, Newmark–β time integration scheme in conjunction with a choice between one of three (2 quasi–Newton an one modified Newton–Raphson) iterative matrix reduction procedures, based on the Green–Nagdhi stress rate formulation. The method is stable for a broad range of nonlinear probelms involving finite strains and (arbitrarily) large rotations. A line search is used with the iterative step that is combined with automatic matrix stiffness reformation to avoid nonconvergence.

Initial and boundary condition prescriptions are flexible. Virtual mass, inertial influences, localized nodal loading, exterior pressure distributions and time histories, surface and internal shear boundary conditions, internal temperature sources, distributions, and conduction and thermal material property changes are all provided together with a self–consistent Jaumann stress rate formulation and a variety of constitutive relations, for generality. In addition, slide line logic (or slide surface logic in the three dimensional studies) permits treatment of discontinuous internal material layers and imbedded material discontinuities, in these simulations.

Concentrated displacement inertial nodal mass loading permits automatic evaluation of added mass effects but with some penalty in computing efficiency, since the

consistent mass matrix formulation requires incremental re-evaluation at every stage of elemental displacement. Since we are also interested in studying the effects of submergence infuences (overburden and temperature) on material response, we choose a simpler, less time-consuming, but equally valid approach. We simply apply a "thin" layer of water over the coating surface to generate shallow, depth added mass inertial influence on surface deflection response. "Thin" here refers to the relative fractional depth of this water overlayer with respect to the underlying depth of coating material (typically 1/5 or less). This provides adequate "coverage" to model coating surface deflection added mass inertial influences without incremental re-evalution of the mass matrix. Of course in our depth of submergence studies, discussed later, the layer of ocean water covering the coating was deepened appropriately for imposition of consistent, static overburden as well as added mass influences.

Material Models and Flow Condition

Of the six general classes of material models available in the finite element codes,[9,10,11] our analyses here are all based on the use of only two: elastic and linear visco-elastic. Fig. 1 illustrates the general flow and material model geometry. While we have examined[12] single layer and multi-layered combination compliant coatings consisting of natural rubber, foams, RTV silicone rubber, polyurethane and other materials, we are presently concentrating on promising combinations of basically two materials. The softest, most yielding of these is polyvinylchloride (PVC). This is a time-cured, gelatinous, visco-elastic material whose shear modulus may vary by one or more orders of magnitude with small changes (a few percent) in the ratio of the polymer to its binder and filler. The other, stiffer material is the more nearly elastic Neoprene, which is conceptually used as an overlayer and for supporting internal structures in the compliant coating candidates discussed here.

Figure 1 represents a modeled planar panel of coating material flush mounted in a semi–infinite flat plate (symbolized by the dashed lines extending indefinitely streamwise). The cartesian coordinate orientation for two–dimensional (x,z) and three–dimensional (x,y,z) computations are sketched at the top of the figure together with the mean potential flow, U_∞, orientation. Streamwise coating lengths ranging from 12 cm to 60 cm and spanwise widths from 5 cm to 12 cm (for three–dimensional computations) have been considered. Total coating depths of from 2 to 8 cm have been studied. Panel locations for the application of uncoupled (surface excitation) or fully fluid/solid interactively coupled pressures establish the finite element streamwise and spanwise nodal spatial distribution. From 10 to 64 streamwise elements and from 3 to 5 spanwise elements have been used while the in–depth distribution of elemental spacing varies from 3 to 12 elemental segments in our computations. The two–dimensional plane–strain computations simulate a vertical cut in a semi–infinite span of coating materials while the three–dimensional computations incorporate finite span and spanwise edge influences. Streamwise and spanwise edge boundary conditions tested included periodic, fixed (adherent), or vertically free (end roller) designations. The base of the coating panel was modeled with a rigid constraint, when it was found that the modeled results were identical using either this simple designation or an actual nearly rigid metal surface (steel) elemental substrate layer.

We have computed results for mean flows of: 1.0, 1.52, 3.0, 10.0, and 30.0 m/s at depths from "ocean surface" (submerged to a depth of about 1/5 to 1 coating depth thickness) down to 200 m with static depth overburden and temperature variations included as initial/boundary conditions.

Two classes of compliant coatings, each combining both materials, Neoprene and PVC, are studied here. One consists of a thin, homogeneous overlayer of the stiffer Neoprene (shown darkened in Fig.1) over the softer PVC underlayer. The Neoprene

overlayer thickness in our calculations varied from 1/5 to 1/10 the thickness of the underlaying PVC. The second class of compliant coatings also uses the thin Neoprene overlayer but includes internal structure consisting of spanwise rectangular slots with a slot depth (or height) about 1/3 of the PVC layer thickness and breadth or width varying over range varying from 1/2 to 4 times the slot depth. Neoprene sidewalls, conceptually separated and supported the unbedded slots. Computations included considerations of slots filled with water, with PVC gel, or empty slots (voids).

The viscoelastic shear modulus of the Neoprene and PVC are modeled by a standard linear time (t) relaxation procedure for linear solids[11] represented by,

$$G(t) = G_{\infty} + (G_0 - G_{\infty})\, e^{-Bt} \tag{3}$$

in which G(t) is the composite shear modulus, while G_{∞} and G_0 are long and short interval shear moduli, respectively, and B is the relaxation frequency parameter.

Figure 2 illustrates the experimentally based (and analytically fit) dependence of the shear modulus on frequency for the relatively stiff Neoprene at a temperature of at 10°C, and for the much more compliant PVC at 10°C and softer yet at 20°C. The dependence shown closely correlates the experimental values reported by Hunston[13] and Gad-El-Hak[14]. The density of the PVC varied, in our model, from 500 to 1025 Kg/m^3, depending on the polymeric percentage in the composition mix. The Neoprene mass density was assumed constant at 1250 Kg/m^3. Both Neoprene and PVC are essentially incompressible with a poisson ratio, ν=1/2. The bulk moduli of the PVC and Neoprene were set at 620 and 5270 MPa respectively, in the model.

Screening Non-interactive "Monte-Carlo" Pressure Exicitation

Materials, composites and internally structured coatings need to be screened and reduced in number so that more exacting coupled computer simulations and experiments

can be limited to a practical number. Our screening procedure makes use of an existing Monte-Carlo turbulent pressure excitation computer model that can be "patched" for boundary conditions to detailed finite element representations of the coating response. Ash[4] and Ash and Khorrami[5] have developed a Monte-Carlo procedure for modeling turbulence pressure excitations on a flat plate. Statistical turbulent functions are simulated that are consistent and convergent to within arbitrarily close representation of experimental measurements.[15]

To initiate a calculation of the turbulent pressure we consider the flow geometry over a flat plate with zero pressure gradient, immersed immediately below the surface in sea water. We examine conditions over a range of specified steady state free stream velocities. The turbulent field development is completed following transition over a specified model transitional length. Also specified is the minimum turbulent structure wavelength of interest. The Ash code generates only a random space and time varying pressure. Convection and convection-dominated burst-streak growth and upthrust vorticity boundary layer features are separately imposed as model parameters.

Figure 3 shows the Ash model results on a Fourier transformed pressure frequency spectra, for a modeled 10 m/s ocean water flow at a spatial position 25% from the leading edge of flat plate which is 0.32 m long. The calculation used a specified transition length, upstream of the model compliant panel leading edge, of 0.50 m.

Time and space scales to be resolved with the pressure model calculations are dictated by the desired structural frequency response range we wish to examine. This range is controlled by finite elemental nodel spacing, material properties of the coating, the presence or absence of voids, and the overall panel dimensions.

Once the pressure patch statistics, particularly the power spectra and decay functions, are checked and found to be reasonable representations of experimental

pressure distribution histories these statistics are saved on disk. The same excitation model is used to stimulate the response of many selected coating panel candidates using identical space and time scales.

Interactive Fluid/Coating Coupling With the Full Navier–Stokes Equations

In this phase of our analysis, the solid material response calculations are simulated using the Hallquist 2- and 3-dimensional finite element computer code methods.[9,10,11] Initially we are concentrating our efforts on examining material coatings that may delay transition to turbulence by reducing the effects of laminar instabilities at sub-transitional Reynolds numbers.

Our current studies impose single wave Tollmein–Schlichting instabilities on a Blasius flow profile, extending from a level coating surface to a mid-plane region that is outside of the significant viscous boundary layer influences.

Our primary consieration here is to develop and apply a method for efficiently and interactively coupling a pseudo-spectral Navier–Stokes simulation of the unsteady, transitional boundary layer flow past a compliant surface represented by finite-element description. Our fluid dynamic procedure uses a modification of the FLOGUN code,[8] which is based on the channel flow procedures by Orszag and his colleagues.[6,7] Surface displacement rate is imposed as a boundary condition for the velocity of the fluid at the wall. These displacement rates are passed to the fluid case incrementally from the finite element code. The fluid code computation, in turn, is used to determine the cyclic variations in pressure distribution that drive the wall. The interactive coupling proceeds indefinitely using either direct or implicit time-step increments. The equations describing the flow field are the incompressible Navier–Stokes equations.

$$\frac{\partial \underset{\sim}{v}(\underset{\sim}{x},t)}{\partial t} + \underset{\sim}{v}(\underset{\sim}{x},t)\bullet\nabla\, \underset{\sim}{v}(\underset{\sim}{x},t) = -\nabla p(\underset{\sim}{x},t) + \upsilon\nabla^2\underset{\sim}{v}(\underset{\sim}{x},t)\ , \qquad (4)$$

and the incompressibility condition,

$$\nabla \cdot \underset{\sim}{v}(\underset{\sim}{x},t) = 0 \tag{5}$$

where $\underset{\sim}{v}$ is the velocity, and $\underset{\sim}{x}$ is the position in two–dimensional space. We have also introduced p, the pressure, (divided by the density), and ν, the kinematic viscosity. The domain of integration is given by

$$\begin{aligned} 0 \leq x \leq X \, , \\ 0 \leq z \leq \infty \, , \end{aligned} \tag{6}$$

with periodic boundary conditions in the x–direction (the horizontal direction) and free–stream inviscid, potential flow boundary conditions at $z = \infty$. We impose the free–stream boundary conditions at a normal distance from the wall approximately five times the local boundary layer thickness. At the wall, the tangential velocity is zero, while the normal velocity is equal to the displacement rates given by the finite element results for the wall motion. For simplicity, this boundary condition is imposed at $z = 0$. The velocity is considered a smoothly varying function and is represented by a truncated series expansion in spectral space.

$$\underset{\sim}{v}(\underset{\sim}{x},t) = \sum_{|m|<M} \sum_{p=0}^{P} \underset{\sim}{u}(m,p,t) \exp[2\pi i m x/X] \, T_p(z) \, . \tag{7}$$

Here $T_p(z) = \cos(p \cos^{-1} z)$, the Chebyshev polynomial of degree p. Using Chebyshev polynomials in the direction normal to the wall results in good resolution in the boundary layer, with about one third of the collocation points being clustered there. Efficiency is gained by evaluating spatial derivatives in spectral space then transforming back to physical space for evaluation of the non–linear advective products. Since the Chebyshev expansion is equivalent to Fourier expansion on a distorted space, fast Fourier transforms

can be applied either to the normal-to-the-wall transformation between Chebyshev space and physical space or the parallel-to-the-wall transformation between Fourier space and physical space.

Time evolution is accomplished in three steps with, for example, the vorticity evaluated in spectral space, then transformed to physical space. The $\underset{\sim}{v}x\underset{\sim}{\omega}$ contribution is evaluated in physical space. This step is performed explicitly in time, with an Adams-Bashforth method.

Development of specialized velocity/pressure boundary conditions and algorithums for the coupled fluid/solid interface flow are described separately in a current publication,[16] so that we will not dwell on them here. Results of these coupled studies indicate that a substantial amount of the disturbance wave energy is transferred, in-phase, to the solid where it is absorbed in resonant, displacement-convection process, in phase with the advected flow disturbance. This flow-solid boundary interaction event is in contrast to coincident fluid/solid dispersion processes which are justifiably receiving considerable attention.[8,13,14] The coupled simulations, of course, involve both convective and dispersive (as well as static) influences generally. It remains an important part of our task to unravel and identify these separate effects in our present and continuing analysis.

III. Discussion of Results

This discussion emphasizes new and different results and suggestions about compliant coating candidates in comparison to our previous summary.[12] In particular, we address here: the special influences of fully three dimensional geometries vs two dimensional plane strain results, the significant influences of added mass and depth overburden in comparison to our previous in-vacuo results, multicomponent layered

coatings including the ordered sequence of materials and layer thickness, and internally structured coatings including considerations on aspect ratio of the cavities and the influence of cavity fillers.

Three Dimensional vs. Two Dimensional Results

The spanwise edges of the compliant surface panel may be considered partially or fully constrained within a flat plate cavity in analogy with a physical flow experiment. The constraint, or lack of it, alters the character of the disturbance waves that are reflected from these boundaries, and significantly alters the response time histories of the coating candidates from the values developed using a strictly two–dimensional, plane strain analysis. In addition, the boundary layer flow itself possesses substantial spanwise inhomogenieties in flow structure.

Using the non–interactive Ash–Khorrami[4,5] Monte–Carlo turbulent pressure model, a one–dimensional streamwise space/time varying pressure "strip" is generated for exciting the two dimensional (finite length and finite depth, infinite span) plane strain results. For our three dimensional panel, parallel "strips" are applied along adjacent rows of elements. The adjacent strips are considered to be statistically independent, that is, spanwise uncorrelated. This is physically analogous to assuming that each row of elements is populated with surface microphones along its length (the pressure sensitive surface "nodes" of the individual finite elements), yet laterally separated at a modest but finite distance from each other that is greater than the spanwise correlation length scale of the turbulent pressure field represented.

To illustrate the general influences of the three–dimensional panel results we first present two–dimensional surface deformation response spectra in Fig 4 for a 10 m/s ocean water flow in zero mean pressure gradient over a 3 cm thick panel of polyvinylchloride (PVC).

Three–dimensional results for this flow condition and coating, using spanwise unconstrained (free surface edge) panel edge conditions, is shown in Fig. 5. Volumetric propagation and reflection of the disturbance waves from finite span extent together with three–dimensional material deformations are seen to modulate and interactively reduce the deformation amplitude and response frequency content at the higher frequencies (much as a low pass filter applied to a partially damped inertial system).

In practice, the two–dimensional plane strain simulations are used for the primary part of the material model and structural screening. The three–dimensional results continue to be reserved for estimates on three dimensional geometrical and flow structure influences on a limited number of the more promising candidates because of their much greater cost and analytical complexity.

Overburden and Added Mass

We tested and isolated the influence of added mass (water inertia) on our surface response computations and evaluated the results in comparison to in–vacuo response results for a 10 m/s ocean water flow. We compare in–vacuo displacement spectra, Fig. 6, with added mass results in Fig. 7. These plane strain, 2D tests were computed for the midplane position on a test panel of PVC assumed to be 1 cm thick. The added mass effects reduce the response to negligible levels in the intermediate range, 60 to 100 Hz, and somewhat modulate the results at even lower frequencies. At higher frequencies yet, the influence of virtual mass is not influential and at about one kilohertz is undetectable, as linear resonance analysis suggests. However, since our attention here is specifically on the frequency band from 1 Hz to about 200 Hz surface response, we include added mass influences in all of our current and future simulations on the surface coating response.

Another important influence that must be considered in analysis of compliant coatings for submersible applications is the effect of ocean depth. Unlike the added mass

inertial correction, submergence to great depth with a compliant coating over a rigid substrate effectively pre-stresses the material to a level necessary to equilibrate the hydrostatic overburden of the water. In effect, the same hydrostatic overburden that applies a crushing force to submersible hulls, stiffens the softer compliant coatings with pre-stress loadings that approach or exceed their elastic moduli. The test calculations here were initiated at an internal material stress state equivalent to the overburden (depth) condition of interest. Amplitude, wavelength and frequency shifts were computed as a function of overburden. The influence of temperature (cooling) at ocean depth on material properties was also tested but found to be negligible with respect to the overburden influences.

The overburden stiffening with depth was found to result in a monotone decreasing value of the root mean square amplitude of coating normal deflection ratio $(\Delta/\Delta_0)_X$ for both Neoprene and softer PVC coatings. As anticipated, the effect of depth is greater for the softer, lower elastic modulus material, PVC, than for the stiffer coating, Neoprene, as seen in Fig. 8. The influence of depth on the band width of a significant portion of the frequency response of PVC coating is shown in Fig. 9. The bandwidth here is that frequency range of the deformation spectrum in which 90% of the significant deformation occurs. The corresponding influences on the much stiffer material, Neoprene, were so insignificant that they were not plotted here.

Layered Homogeneous Coatings

The thickness of the compliant coating is a significant factor in response amplitude, whether it appears as a single layer or part of a multiply layered coating over a stiff substrate. Increasing thickness, however, is not, by itself, a positive influence on desirable compliant coating response, since a too-thick depth of coating can be a factor leading to the onset of static divergence.[13,14] The resulting larger amplitude surface

deformations generally occur at very low frequency, which, as in the static divergence case, may offset drag reduction, and may, in fact, increase the drag.

Our results, however, show that use of ordered multilayer coatings may produce the sought for results on controlled small amplitude deformation at substantial frequencies. This is particularly true with a thick (1 cm to 2 cm) layer of soft material (PVC) over which is placed a much thinner (2 mm) coating of a stiffer material (Neoprene). The results at a mean flow speed of about 10 m/s appear encouraging using such composite multilayer coatings in our simulations.

Internally Structured Coatings

Our analysis on internally structured coatings, to date, has been restricted to coatings with internal reinforcing stiffeners and channeled openings that are oriented transverse (spanwise) to the mean flow direction in the coating. We have examined both liquid filled and empty (void) channels using a viscous liquid (PVC) and an incompressible liquid (water) as a filler in comparison to open, coating–imbedded, channels (voids). The voids yield the most promising results in terms of rms and peak response amplitudes to surface pressure excitation.

Shallow but wide channels, particularly for voided (no filler) cases, with channel width to height of 3 or more also show the most promise for coating response amplitude enhancement as seen in Fig. 10. Our simulations incorporate the thin outer stiffened layer of firmer material as an upper layer to the stub supported channels within a thick layer of the low modulus PVC material. Excitation induced frequency response of the structured coatings is also much more satisfactorily reproduced over a broad range of excitation frequencies when voids rather than liquid filler are used.

IV. Summary

Some preliminary indications apparent from our numerical studies at this time, are summarized.

- Added mass and depth of submergence (overburden) considerations must be included in analysis of compliant coating performance, particularly for the softest, lowest moduli materials, which dynamically respond as if they were much stiffer materials when those influences are included in our computations.
- Composite multilayered coatings show promise for drag reduction, particularly when thickened soft inner coating layers are sandwiched between a stiffer thin outer coating layer and a rigid substrate.
- Shallow flat channels imbedded in the material and oriented transversely (spanwise) to the mean flow direction may favorably modulate amplitude, frequency and wavelength of the response, particularly if the channel is left open, free of filler material.
- Three dimensional influences of both the flow patterns and the compliant surface geometry should be evaluated and corrected for, prior to recommending promising coating candidates for further experimental verification.

Acknowledgment

It gives us great pleasure to acknowledge the substantial contributions in the form of advice and corrective suggestions supplied to us by our LLNL colleagues L. A. Glenn, J. O. Hallquist, and J. Levatin. It is also a pleasure to acknowledge the rapidity, accuracy, and expertise applied to the timely production of the original MS by K. Smith.

V. References

1. Kramer, M. O., "Boundary Layer Stabilization by Distributed Damping", J. Amer. Soc. of Naval Engrs. 72 (1) 25–33 (February, 1960).

2. Kramer, M. O., "Dolphin's Secret", The New Scientist, London, 7 (181) 1118–1120 (May, 1960).

3. Kozlov, L. P., V. I. Korobov, V. V. Babenko, "The Effect of an Elastic Wall on a Boundary Layer", Reports of Ukranian Academy of Sciences, Series A: Physical, Mathematical and Technical Sciences, 45–47 (January, 1983).

4. Ash, R. L., Simulation of Turbulent Wall Pressures, NASA CR–2958 (May, 1978).

5. Ash, R. L., M. Khorrami, "Simulation of Turbulent Wall Pressure Fluctuations for Flexible Surface Response Studies", AIAA Paper 83–0292, AIAA 21st Aerospace Sciences Meeting, (Reno, Nevada, June 10–13, 1983).

6. Orszag, S. A., L. C. Kells, "Transition to Turbulence in Plane Poiseuille and Plane Channel Flow", Journ. Fluid Mech. 96 (1), 159–205 (1980).

7. Orszag, S. A., A. T. Patera, "Subcritical Transition to Turbulence in Plane Channel Flows", Phys. Review Ltrs. 45 (12) 989–992 (1980).

8. Metcalf, R., T. McMurray, "FLOGUN Pseudo Spectral Turbulent Calculations near Compliant Walls" in Drag Reduction Symposium Proceedings, M. M. Reischman, ed. (National Academy of Sciences, Washington, D.C., September 13-17, 1982).

9. Hallquist, J. O., "User's Manual for DYNA-2D, An Explicit Two-Dimensional Hydrodynamics Finite Element Code with Interactive Rezoning", Lawrence Livermore National Laboratory, Livermore, CA Report UCID-18756, Rev. 1 (1982).

10. Hallquist, J. O., "User's Manual for DYNA3D and DYNAP (Nonlinear Dynamic Analysis of Solids in Three Dimensions)", Lawrence Livermore National Laboratory, Livermore, CA Report UCID-19156 (1981).

11. Hallquist, J.O. "NIKE2D, A Vectorized, Implicit Finite Deformation, Finite Element Code for Analyzing the Static and Dynamic Response of 2-D Solids". Lawrence Livermore National Laboratory, Livermore, CA report UCID-19677 (1983).

12. Buckingham, A. C., R. C. Chun, R. L. Ash, and M. Khorrami, "Compliant Material Coating Response to a Turbulent Boundary Layer", AIAA Paper No. 82-1027 in AIAA/ASME 3rd Joint Thermophysics, Fluids, Plasma and Heat Transfer Conference (St. Louis, Mo., June 7-11, 1982).

13. Rathson, A., "Measurement of Plastisol Response to a Turbulent Boundary Layer", in Drag Reduction Symposium Proceedings, M. M. Reischman, ed. (National Academy of Sciences, Washington, D.C., September 13-17, 1982) and personal communication, May, June 1983.

14. Gad-El-Hak, M., R. F. Blackwelder, and J. J. Riley, "Effects of Compliant Coatings on Turbulence and Transition", Proc. IUTAM Symp. on Structure of Complex Turbulent Flow (Marseille, August, 1982), and personal communication, May 1983.

15. Bull, M. K., and A. S. W. Thomas, "High Frequency Wall Pressure Flutuations in Turbulent Boundary Layers", Physics of Fluids 19, 597-599 (1976).

16. Hall, M. S. and A. C. Buckingham, "Calculations of the Interaction Between a Compliant Material and an Unsteady Flow", presented at the XVIth International Congress of Theoretical and Applied Mechanics (Lyngby, Denmark August 19-25, 1984).

1065c

FIGURE CAPTIONS

Fig. 1. Geometry of compliant surfaces, flow and coordinate orientation for finite element transient response simulations.

Fig. 2. Shear modulus of two critical materials as a function of frequency for compliant coating response models.

Fig. 3. Driving pressure excitation spectral distribution from the Ash Monte–Carlo model (Refs. 4 and 5) for a 10 m/s ocean water flow at a position 25% from the leading edge of a 0.32 m flat plate compliant surface.

Fig. 4. Fourier transformed displacement vs frequency distribution for the response at the mid–panel position of a 3 cm thick PVC panel in two–dimensional flow at 10 m/s.

Fig. 5. Fourier transformed displacement vs frequency distribution for the response at the mid–panel position of a 3 cm thick PVC panel in three–dimensional flow at 10 m/s.

Fig. 6. Fourier transformed displacement vs frequency distribution for the response at the mid–panel position of a 1 cm thick PVC panel in a two–dimensional flow at 10 m/s.

Fig. 7. Fourier transformed displacement vs frequency distribution for the response at the mid–panel position of a 1 cm thick PVC panel including added mass in a two–dimensional flow at 10 m/s.

Fig. 8. Ratio of root-mean-square surface displacements at depth to displacements at sea level as a function of depth for 3 cm thickness Neoprene and PVC coating panels at the mid-channel position.

Fig. 9. Band width of mid panel PVC 90% displacement response as a function of ocean depth for a 3 cm thick PVC panel in 10 m/s flow.

Fig. 10. Root-mean-square surface displacements at the mid-panel position of 3 cm thick internally channeled panel in 10 m/s flow as a function of width/height aspect ratio and channel filler.

Fig #1

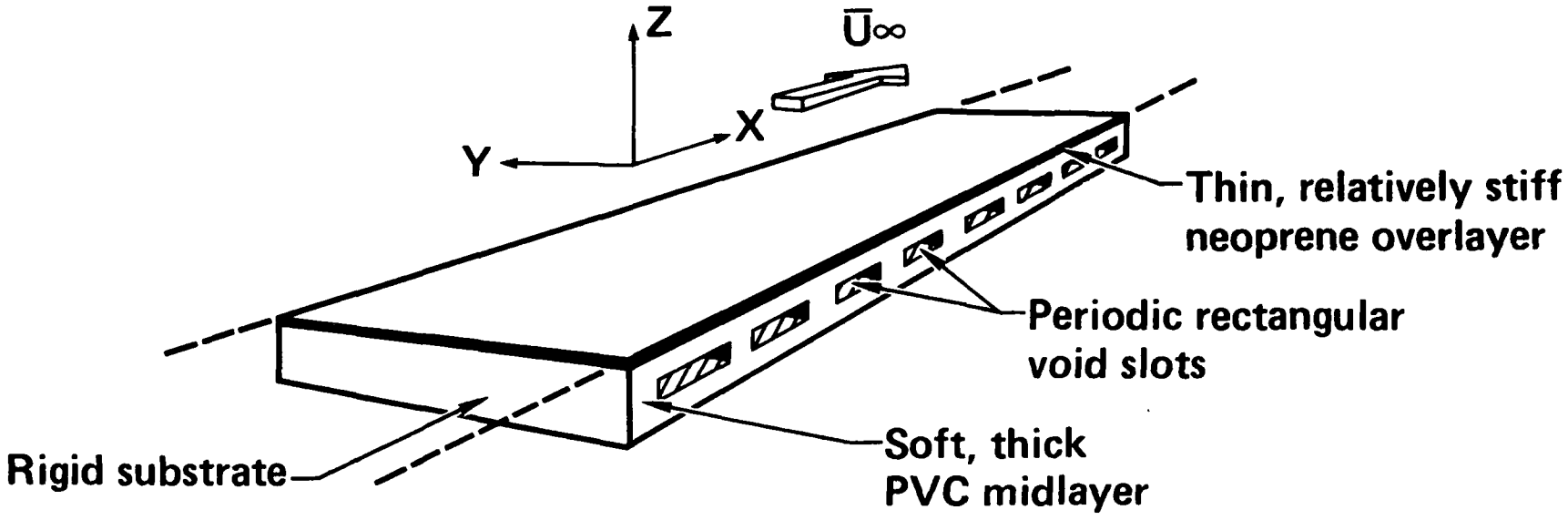
Z
$\bar{U}\infty$
X
Y
Thin, relatively stiff
neoprene overlayer
Periodic rectangular
void slots
Soft, thick
PVC midlayer
Rigid substrate

Fig. #2

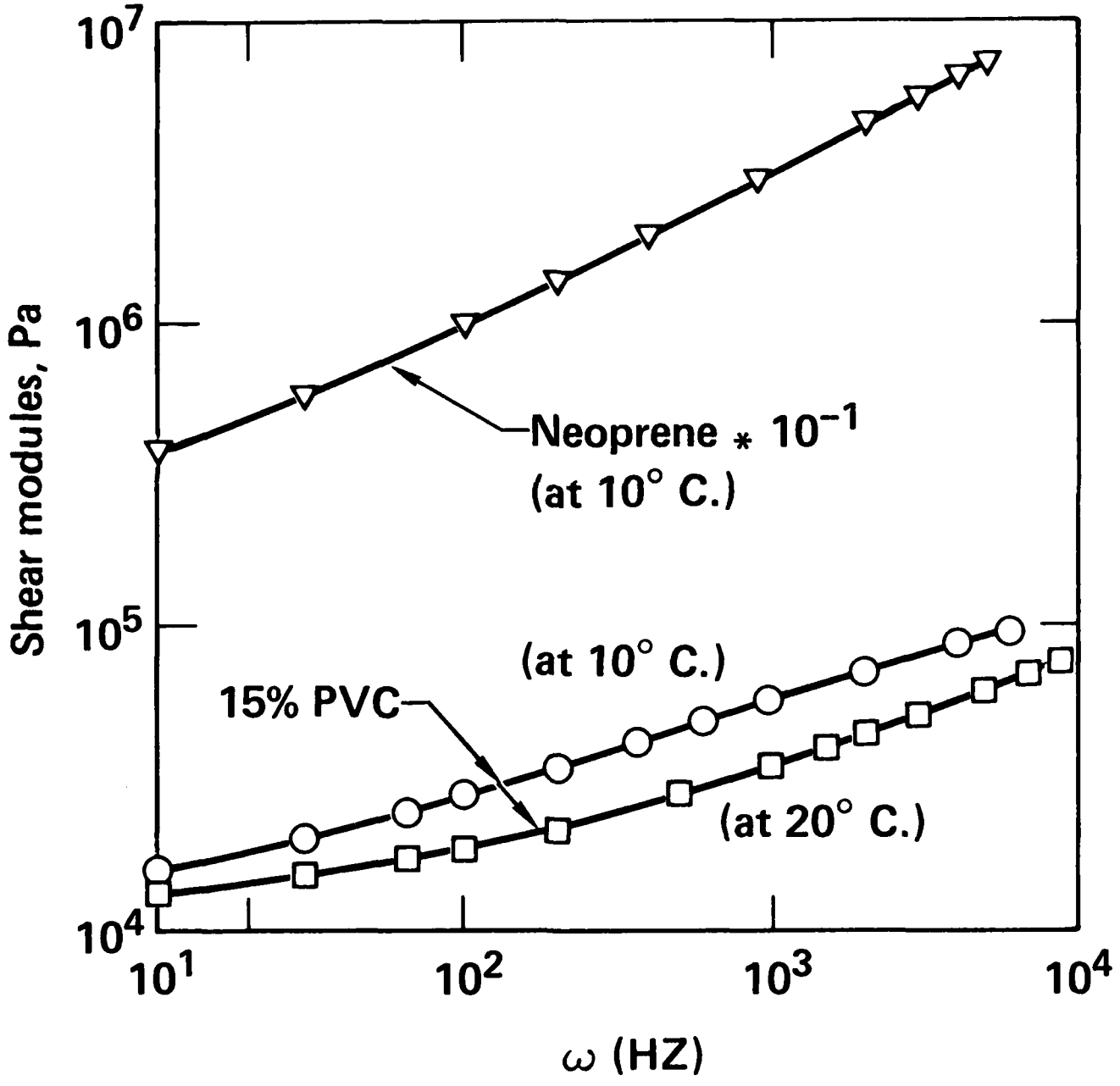
10^7
10^6
10^5
10^4
Shear modules, Pa
Neoprene * 10^{-1}
(at 10° C.)
(at 10° C.)
15% PVC
(at 20° C.)
10^1
10^2
10^3
10^4
ω (HZ)

Fig #3

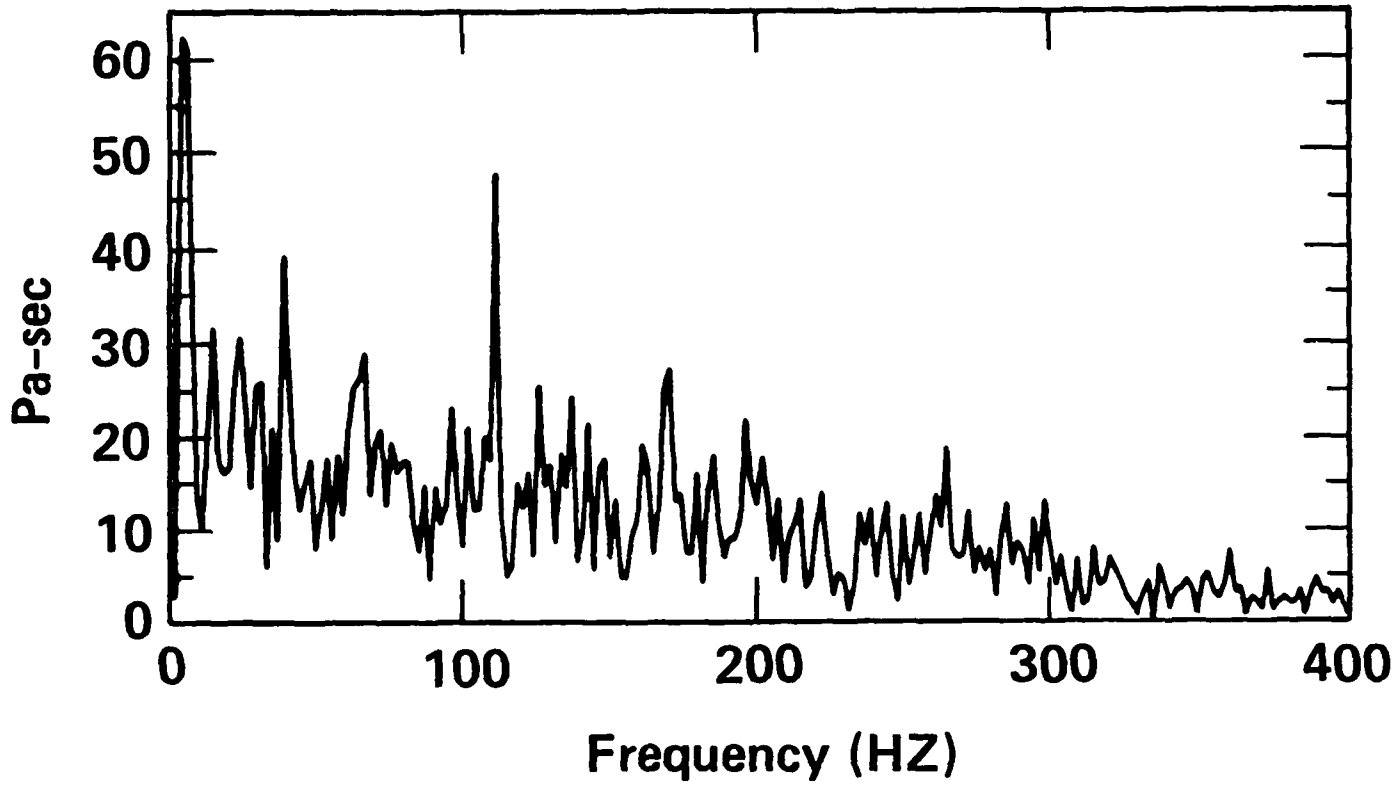

Fig. #4

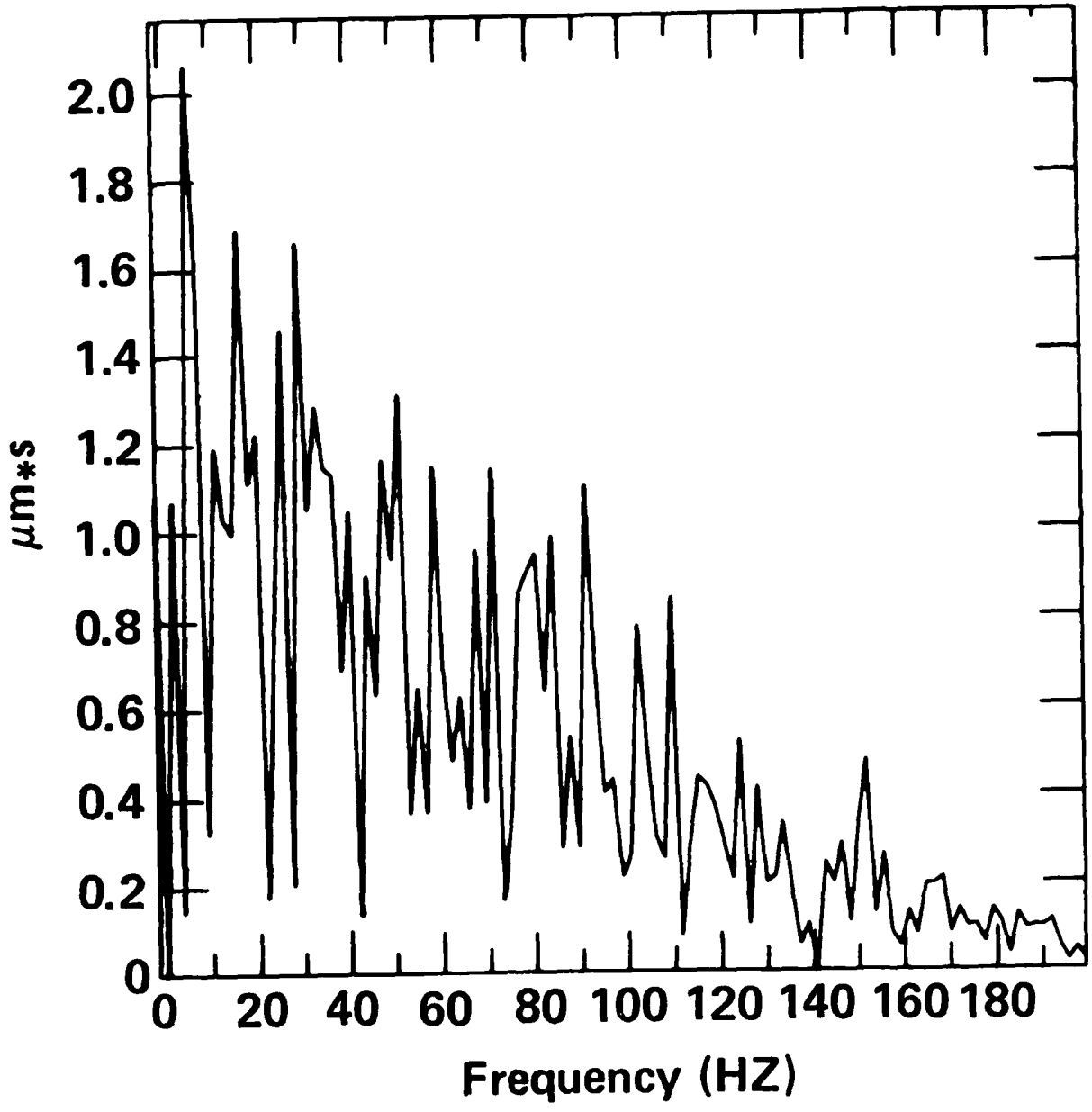
2.0
1.8
1.6
1.4
1.2
1.0
0.8
0.6
0.4
0.2
0
μm*s
0
20
40
60
80
100
120
140
160
180
Frequency (HZ)

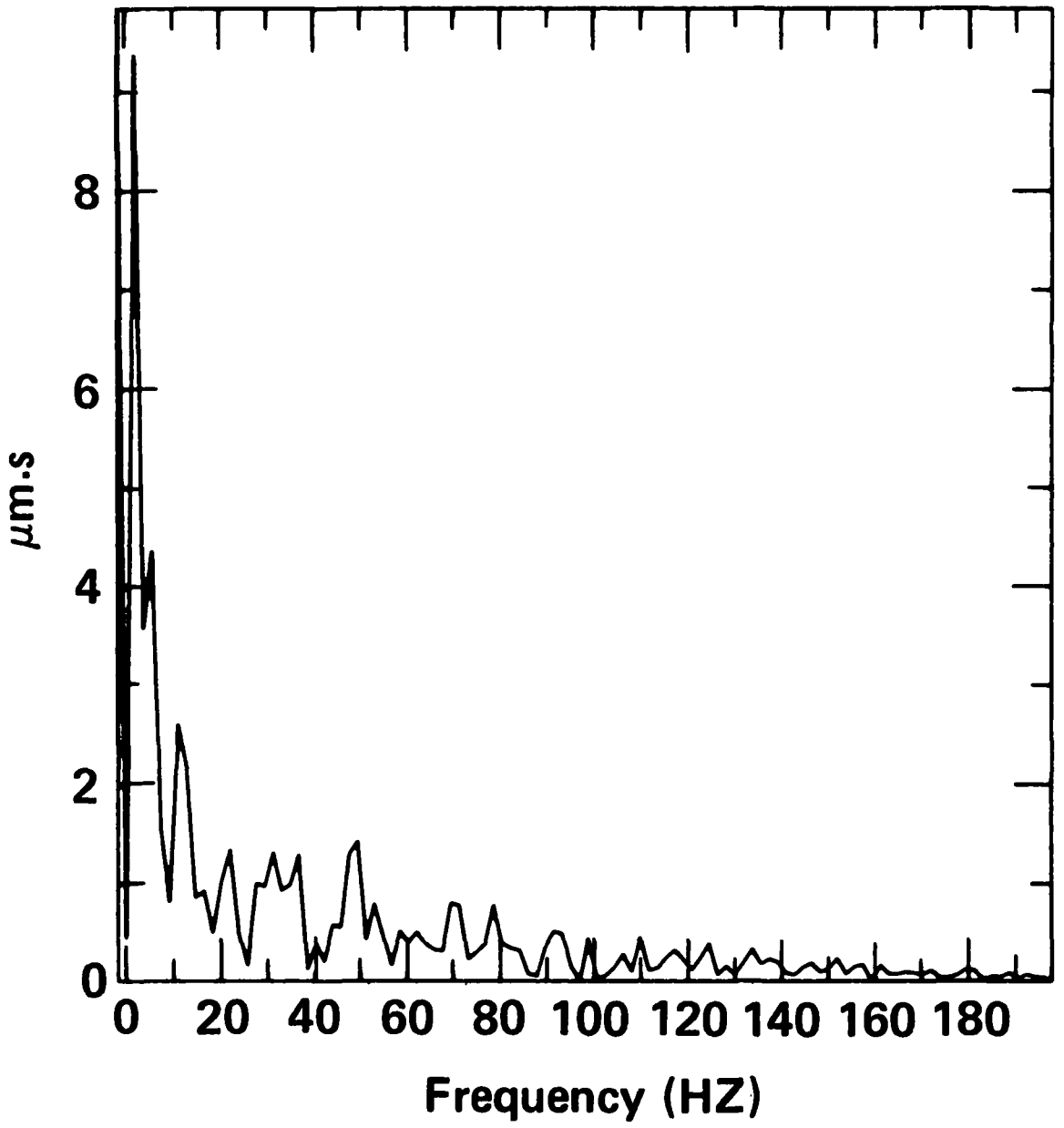
8
6
4
2
0
μm.s
0 20 40 60 80 100 120 140 160 180
Frequency (HZ)

Fig # 6

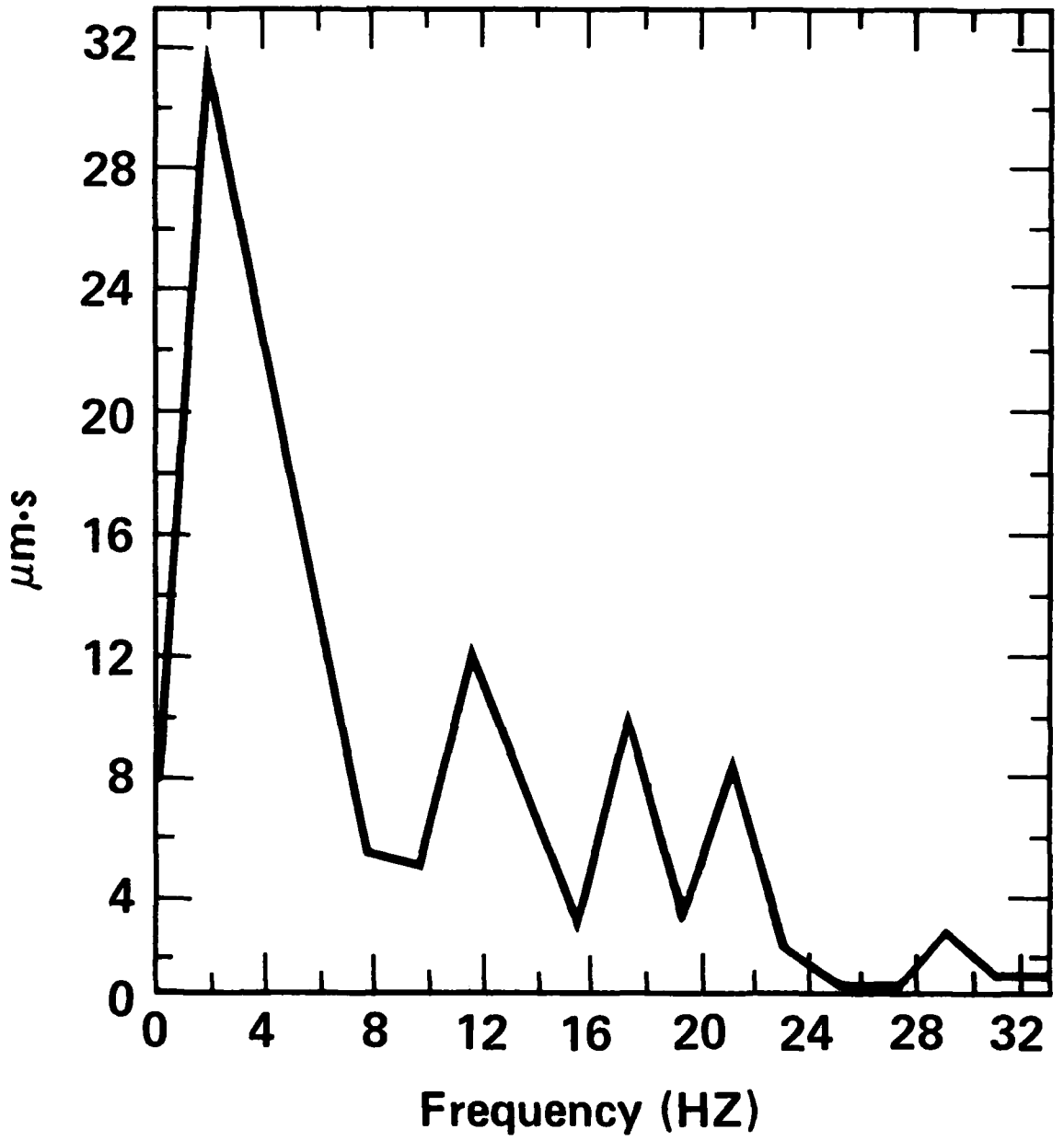

Fig. #7

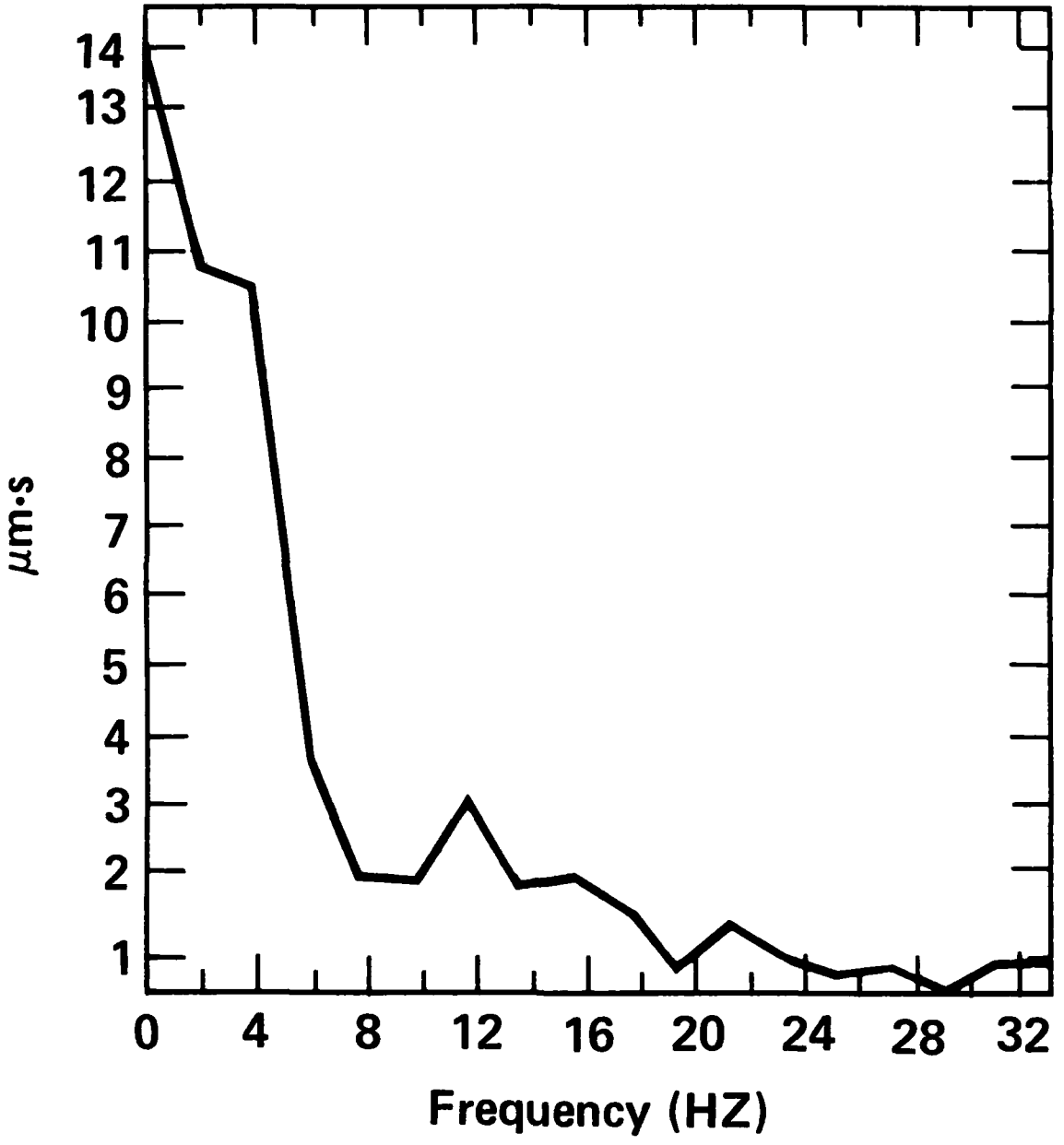

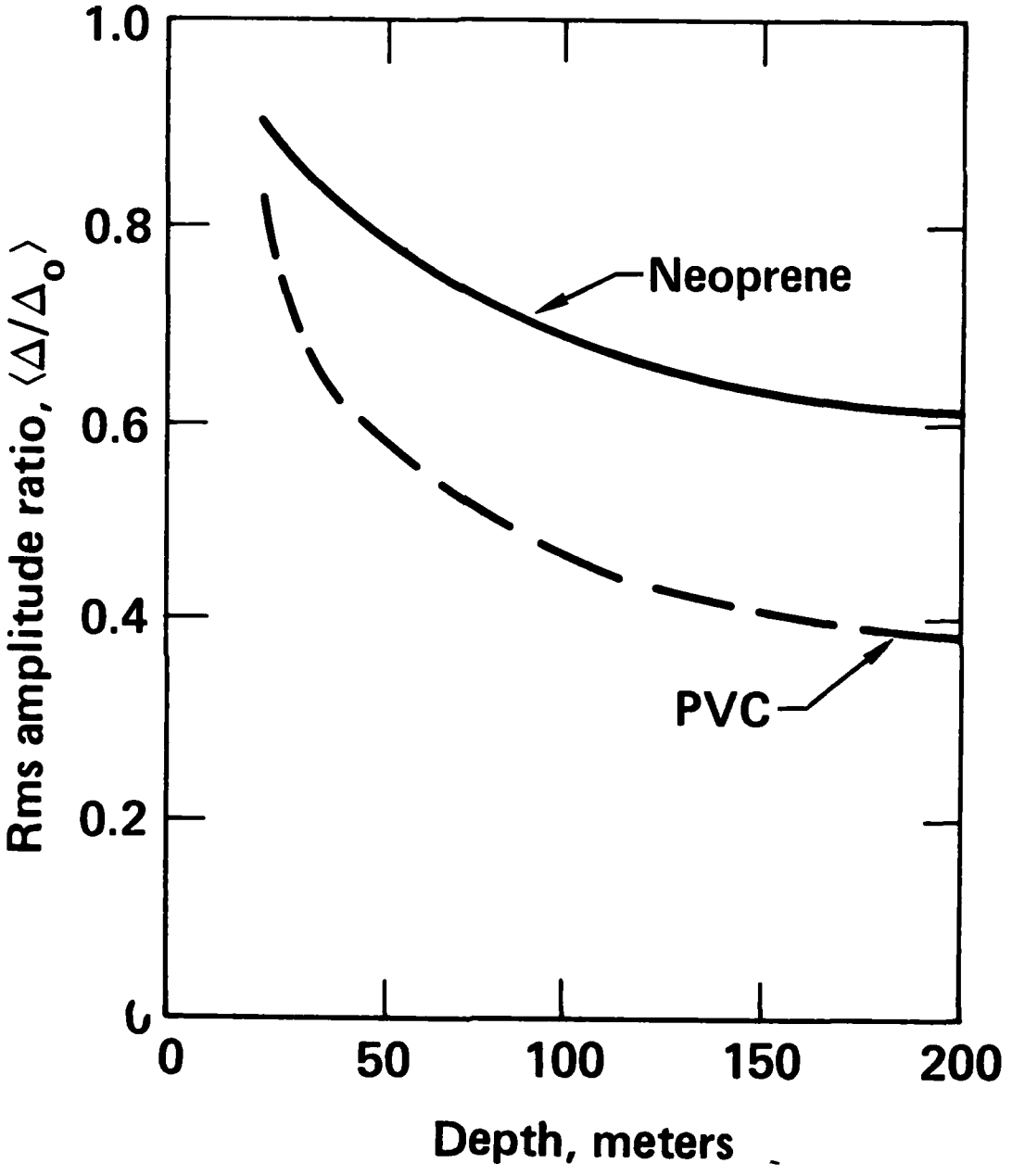
1.0
0.8
0.6
0.4
0.2
0
Rms amplitude ratio, $\langle \Delta/\Delta_o \rangle$
Neoprene
PVC
0
50
100
150
200
Depth, meters

Fig #9

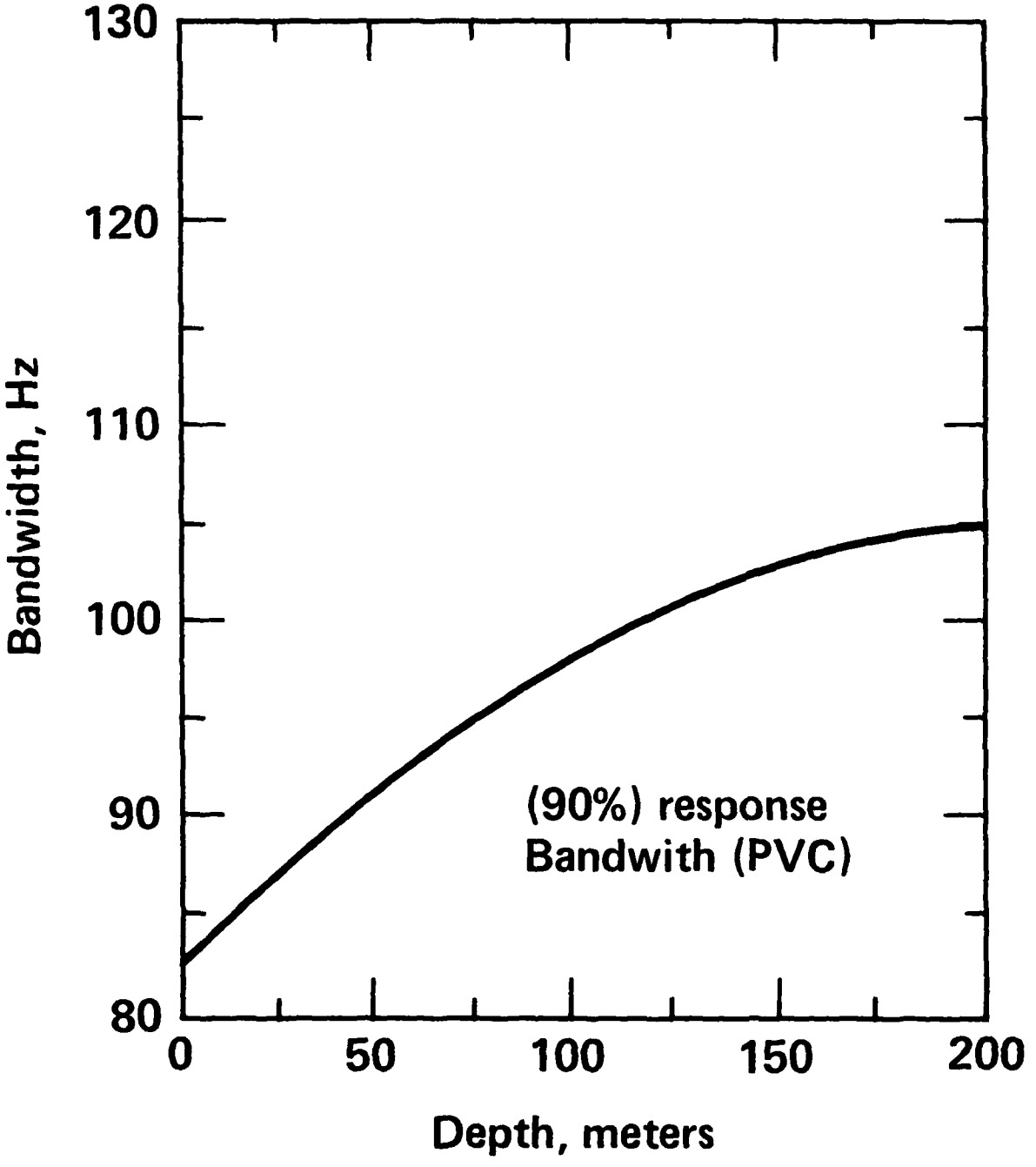
130
120
110
100
90
80
Bandwidth, Hz
(90%) response
Bandwith (PVC)
0
50
100
150
200
Depth, meters

#10

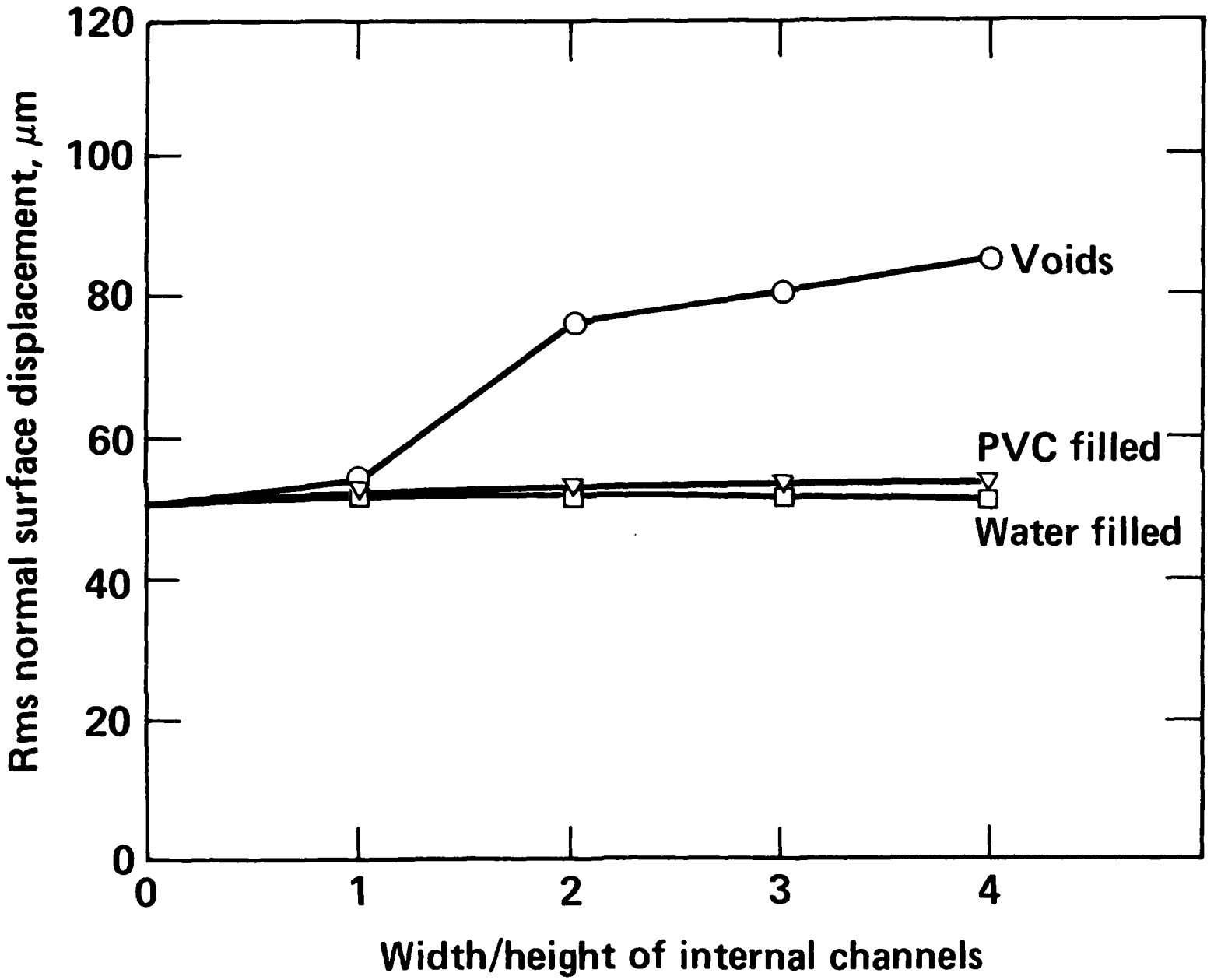
120
100
80
60
40
20
0
Rms normal surface displacement, μm
Voids
PVC filled
Water filled
0
1
2
3
4
Width/height of internal channels